Preferred Hierarchical Control Strategy of Non-Point Source Pollution at Regional Scale

Weijia Wen
Chinese Academy of Sciences Innovation Academy for Precision Measurement Science and Technology
Yanhua Zhuang (zhuang@whigg.ac.cn)
Institute of Geodesy and Geophysics Chinese Academy of Sciences https://orcid.org/0000-0002-7041-1118
Liang Zhang
Chinese Academy of Sciences Innovation Academy for Precision Measurement Science and Technology
Sisi Li
Chinese Academy of Sciences Innovation Academy for Precision Measurement Science and Technology
Shuhe Ruan
Chinese Academy of Sciences Innovation Academy for Precision Measurement Science and Technology
Qinjing Zhang
Wuhan University

Research Article

Keywords: Non-point source (NPS) pollution, Critical periods (CPs), Critical source areas (CSAs), Dual-structure export empirical model, Point density analysis (PDA), Management

Posted Date: February 18th, 2021

DOI: https://doi.org/10.21203/rs.3.rs-193825/v1

Preferred hierarchical control strategy of non-point source pollution at regional scale

Author names and affiliations

Weijia Wen[1,2], Yanhua Zhuang[1*], Liang Zhang[1], Sisi Li[1], Shuhe Ruan[1,2], Qinjing Zhang[3]

[1] *Hubei Provincial Engineering Research Center of Non-Point Source Pollution Control, Innovation Academy for Precision Measurement Science and Technology, Chinese Academy of Sciences, Wuhan 430077, Peoples R China*

[2] *University of Chinese Academy of Sciences, Beijing 100049, Peoples R China*

[3] *School of Resource and Environmental Sciences, Wuhan University, Wuhan 430079, Peoples R China*

Information about the corresponding author

*Yanhua Zhuang

Innovation Academy for Precision Measurement Science and Technology, Chinese Academy of Sciences, Wuhan 430077, Peoples R China

Tel/Fax: +86-27-68881362

E-mail: zhuang@apm.ac.cn

Preferred hierarchical control strategy of non-point source pollution at regional scale

Abbreviations

Non-point source (NPS); Critical periods (CPs), critical source areas (CSAs), point density analysis (PDA), dual-structure export empirical model (DSEEM); total phosphorus (TP), Danjiangkou Reservoir Basin (DRB).

Abstract

Non-point source (NPS) pollution has wide range of sources. Under rainfall conditions, NPS pollution occurs mainly by overland flow, resulting in difficult governance. In this study, based on the cooperative analysis of critical periods (CPs) and critical source areas (CSAs), a preferred hierarchical control strategy of NPS pollution, which was connected with management units, was proposed in the Danjiangkou Reservoir Basin (DRB) to improve the pertinence of NPS pollution control. The practicality of the grid-based CSA identification results was improved by point density analysis (PDA). CPs, sub-CPs, and non-CPs were identified on the temporal scale; CSAs, sub-CSAs and non-CSAs were identified on the spatial scale. The results showed that CPs (July, April, and September), sub-CPs (May, March, and August), and non-CPs contributed 62.8%, 31.1%, and 6.1% of the annual TP loads, respectively. Furthermore, we proposed a hierarchical NPS pollution control strategy: class I (CSAs in CPs) → class II (sub-CSAs in CPs, CSAs in sub-CPs) → class III (non-CPs, non-CSAs, sub- and non-CSAs in sub-CPs). Class I covered the periods and areas with the highest NPS pollution loads, contributing 26.2% of the annual load within 14.5% of the area and 25.0% of the time. This study provides a reference for the targeted control of NPS pollution at regional scale, especially in environmental protection with limited

funds.

Keywords: Non-point source (NPS) pollution; Critical periods (CPs); Critical source areas (CSAs); Dual-structure export empirical model; Point density analysis (PDA); Management

1 Introduction

Non-point source (NPS) pollution is an important source of river and lake eutrophication and is a major factor deteriorating water quality (Le et al. 2010, Ongley et al. 2010, Vander Zanden et al. 2005, Xue et al. 2020). Impacted by topography, land-use, precipitation, vegetation coverage, and other factors, NPS pollution has great spatiotemporal heterogeneity (Yu et al. 2011). Under rainfall conditions, NPS pollution occurs mainly by overland flow, resulting in difficult governance and low efficiency(Tian et al. 2010). Critical source areas (CSAs) and critical periods (CPs) generate disproportionately high pollutant loads of NPS pollution (Bannerman et al. 1993, Sharpley et al. 1993, Zhang et al. 2019). Studies have shown that more than 50% of the load is generated from CPs, accounting for 25% of the time (Ruan et al. 2020), and more than 50% of the load is generated form CSAs, accounting for less than 30% of the area (Gburek &Sharpley 1998, Liu et al. 2016b, Zhuang et al. 2016). Therefore, it is important to identify, target, and remediate the CPs and CSAs to effectively control NPS pollution with limited funds.

The proper identification of CSAs and CPs is crucial. First, model selection affects the precision of identification results and the economic viability of best management practices (BMPs) (Shrestha et al. 2021). In recent years, methods have been proposed for the identification of CSAs along with the development of the NPS pollution model. The export coefficient method is effective in load simulation of large watersheds. However, ignoring the spatiotemporal variation of factors such as runoff and vegetation interception leads to a deviation in CSA distribution (Ding et al. 2010, Johnes 1996, Wang et al. 2020). The mechanistic models (e.g., soil and water assessment tool), which can simulate the characteristics of pollutant transport, can reflect the actual distribution of CPs and CSAs. However, large amounts of high-quality data are required for model calibration and verification (Hao et al. 2004, Panagopoulos et al. 2011, Soranno et al. 1996). The dual-structure export empirical model (DSEEM)

simulates pollutant loads in particulate and dissolved states respectively; that is, it has the advantage of a model that accurately describes the process of nitrogen and phosphorus loss and requires fewer data (Shi et al. 2002, Wang et al. 2012). Second, the selection of identification methods affects the objectivity of the results. Some methods, such as the pollution index method (e.g., the P Index), which is a simple and wildly used approach, are often conducted subjectively based on expert recommendations without uniform standards (Drewry et al. 2011, Kaplowitz &Lupi 2012, Lemunyon &Gilbert 1993, Nelson &Shober 2012, Sharpley et al. 2003). Third, differences in the spatial scale affect the identification accuracy of CSA. For large-scale watersheds, most CSAs are identified through sub-catchment units, which is an efficient approach for the identification of CSAs; however, it neglects the heterogeneity of NPS pollution load distribution in sub-catchments (Liu et al. 2016b, Niraula et al. 2013, Pradhanang &Briggs 2014, Ruan et al. 2020, Wang et al. 2018). Considering that administrative units (such as a county) or farms, which are distinct and disconnected with hydrological units, are used for management in most situations (Ghebremichael et al. 2013, Li et al. 2017, Shen et al. 2020), it is difficult to achieve accurate prevention and control of NPS pollution and to effectively allocate BMPs. For small watersheds, CSAs are mostly identified by grids (Zhuang et al. 2016). Grid-based identification can reveal the relationship between the spatial distribution of pollutant load and regional characteristics (topography, land use type, rainfall, etc.). However, the discrete distribution of some CSAs may lead to poor guidance the results.

In this study, the Danjiangkou Reservoir Basin (DRB), an important water source for the Middle-Route of the South-to-North Water Diversion Project of China (Nong et al. 2020), is selected as the study region to propose a preferred hierarchical NPS pollution control strategy of spatiotemporal pertinence. The main objectives of this study are to (1) simulate the spatiotemporal distribution of the total

phosphorus (TP) load based on the DSEEM at a monthly scale; (2) conduct a cooperative analysis of the CPs and CSAs; (3) extract CSAs with more realistic guiding importance by point density analysis (PDA); and (4) propose a hierarchical control strategy for NPS pollution.

2 Materials and Methods

2.1 Study area and environmental database

The DRB (109°29′–111°53′E, 32°14′–33°48′N) is located in the middle and upper reaches of the Hanjiang River Basin at the junction of Hubei and Henan provinces (Fig. 1). The total area is approximately 17,924 km^2, including Danjiangkou City, Shiyan City, Xichuan County, Yunxi County, Yunxian County, and Xixia County. The altitude of the DRB is 17–2125 m, and the overall terrain is high in the northwest and low in the southeast (Fig. 1c). The topography is dominated by hills and mountains, accounting for approximately 97% of the area (Huang et al. 2012). The average annual rainfall of 800–1000 mm is distributed unevenly, mainly from June to September, with rainfall in July accounting for approximately 20% of the total annual rainfall.

[Insert Fig. 1 here]

Phosphorus is a limiting factor for water quality in the DRB (Chen et al. 2015). Soil erosion, carrying large amounts of phosphorus in the sediment, is an important factor causing NPS pollution and affecting the water quality of the DRB (Huang et al. 2017, Jiang et al. 2020). Characteristics including steep slopes, time variation of normalized difference vegetation index (NDVI) and rainfall causes a clear spatiotemporal heterogeneity of NPS pollution in this area. (Wang et al. 2020). In addition, agricultural NPS pollution is an important source of water pollution in this area (Huang et al. 2012) due to frequent agricultural activities (mainly farming) a and the overuse of chemical fertilizers and pesticides (Jiang et

112 al. 2010).

113

114 **2.2 Simulation of NPS pollution loads**

115 In this study, we adopted the DSEEM to estimate the monthly TP loads from the perspectives of
116 particulate and dissolved pollutant loads based on the collected environmental data (Table 1) (Shen et al.
117 2010, Shi et al. 2002).

118 **2.2.1 Particulate pollutant load**

119 The particulate pollutant load is calculated as:

120 $$L_s = \alpha \cdot \eta \cdot A \cdot C_s \cdot S_d \quad (1)$$

121 where L_s is the particulate pollutant load (kg/ha/month), α is the transformation coefficient (kg/t), A is
122 the soil erosion (t/ha/month), η is the enrichment ratio of the soil pollutant (dimensionless), C_s is the
123 concentration of particulate phosphorus in soil particles (%), and S_d is the sediment transport ratio
124 (dimensionless). The values of each parameter in the formula were determined based on the background
125 data of the study area and previous studies (Shen et al. 2010, Zhuang et al. 2016). A is calculated using
126 MUSLE model:

127 $$A = R \cdot LS \cdot K \cdot C \cdot P \quad (2)$$

128 where A is the monthly soil erosion amount (t/ha/month), R is the rainfall erosivity factor
129 (MJ·mm/ha/h/month), LS is the slope factor of slope length (dimensionless), K is the soil erosion factor
130 (t·h/ MJ/mm), C is the land cover and its management factor (dimensionless) and P is the soil and water
131 conservation measurement factor (dimensionless).

132

133 **2.2.2 Dissolved pollutant load**

The dissolved pollutant load is calculated as:

$$L_d = \beta \cdot C_d \cdot Q \tag{3}$$

where L_d is the dissolved phosphorus load of ground types (kg/ha), β is the conversion coefficient, C_d is the concentration of pollutants (mg/L), and Q is runoff depth (mm).

Algorithms of all these factors are based on the background information of the study area (Shen et al. 2010). Q is determined using the Soil Conservation Service model:

$$Q = \begin{cases} \dfrac{(P-0.2S)^2}{P+0.8S} & P \geq 0.2S \\ 0 & P < 0.2S \end{cases} \tag{4}$$

$$S = \frac{25400}{CN} - 254 \tag{5}$$

where Q is the runoff depth (mm), P is the rainfall (mm), S is the maximum infiltration (mm), and CN is the number of curves (dimensionless).

2.3 Identification of CPs and CSAs

2.3.1 Cumulative load–time/area curve fitting

Based on the simulation results of the monthly TP load, we adopted the load–time accumulation curve and load–area accumulation curve to identify the CPs and the CSAs of the phosphorus runoff loss in DRB during typical years (Ruan et al. 2020, Zhuang et al. 2016). CPs were given priority because the temporal variability of NPS pollution was greater than the spatial variability in the study area. First, the TP load of each month was arranged in descending order to obtain the data set (l_1, … l_i, … l_m), where l_1 is the maximum and l_m is the minimum value. Then, the cumulative load L_j and cumulative months T_j were calculated as:

$$L_j = \sum_{i=1}^{j} l_i \tag{6}$$

$$T_j = \sum_{i=1}^{j} t_i \quad (7)$$

where L_j is the cumulative TP load under load grade j in a month (t), l_i is the TP load of the *ith* month (t), T_j is the cumulative number of months under load grade j, and t_i is the number of months.

The cumulative percentage of TP load (Pl_j) and the corresponding cumulative percentage of time (Pt_j) were calculated as:

$$Pl_j = \frac{L_j}{L_{total}} \times 100\% \quad (8)$$

$$Pt_j = \frac{T_j}{T_{total}} \times 100\% \quad (9)$$

where L_{total} is the annual total TP load of the study area (t) and T_{total} is the total number of months.

The cumulative load–time curve was fitted by taking Pl_j as the ordinate and Pt_j as the abscissa, with f as the fitting function:

$$Pl_j = f(Pt_j) \quad (10)$$

CSAs were similarly identified. The dataset (l_1, … l_i, … l_n) was generated by arranging the TP load of each grid in a descending order, where l_1 is the maximum and l_n is the minimum value. The relevant parameters were calculated as:

$$Pa_j = \frac{A_j}{A_{total}} \times 100\% \quad (11)$$

where Pa_j is the cumulative percentage of grids under load grade j, A_j is the cumulative number of grids, and A_{total} is the total number of grids.

The cumulative load–area curve was fitted as:

$$Pl_j = f(Pa_j) \quad (12)$$

where f is the fitting function.

2.3.2 Criterion selection of CPs and CSAs

k_t and k_a were the slopes of any point on the curve. For the load–time curve, k_t values indicate the relationship between the growth rate of the TP load and time. When $k_t > 1$, the load grows faster than time, implying that when the time increment is 1%, the load increment is greater than 1%. Here, the value of k_t is 1 as the index to divide the CPs and sub-CPs of phosphorus loss, and the value of k_t is 0.5 as the index to divide the sub-CPs and non-CPs. For the load–area curve, k_a values represent the growth rate of the TP load along the area. Combined with the concentration of the load in the study area, regions with k_a values greater than 2 were divided into CSAs, those with k_a values greater than 2 and less than 1 were divided into sub-CSAs, and those with *k'* values less than 1 were divided into non-CSAs. In addition, the CSAs in the CPs, sub-CPs, and the non-CPs were identified to compare the load contribution of CSAs during different periods.

k_t and k_a values were calculated as:

$$k_t = f'(Pt_j) \tag{13}$$

$$k_a = f'(Pa_j) \tag{14}$$

2.3.3 PDA of CSAs

The identification results of the CSAs based on the grid scale are often discretized, leading to a lack of guidance in the implementation of NPS control measures. Considering the difficulty in management, the environmental quality requirements of surface water and the self-purification ability of water bodies, some discretely distributed CSAs do not need to adopt centralized control measures. Therefore, identification results based on the cumulative load–area curve were processed further in this study. Here, the PDA was employed to describe the distribution density of the original CSA grids, followed by the extraction of high-density areas as CSAs that required critical control. Thus, CSAs too discrete to control were screened out. Few small CSAs scattered around large CSAs with high TP loads (such as large

dryland CSAs), and few areas between them, were also divided into the final CSAs. In addition, by combining the distribution of slope and land-use types in the study area, few CSAs that are remote, difficult to reach, and small in size were screened to improve the practicality of the identification results.

3 Results and Discussion

3.1 Accuracy verification

(1) TP load

The annual total TP loads in the DRB (excluding Shiyan City) in 2010 were 0.29×10^4 t/a, and the TP loads of all six counties or cities in the DRB were 0.30×10^4 t/a. In 2010, the annual TP loads of the DRB were 0.28×10^4 (excluding Shiyan City) (Jiang et al. 2010) and 0.29×10^4 (the entire study area) (Zhuang et al. 2016). Compared with the results reported by (Jiang et al. 2010), who simulated the TP loads with the equivalent pollution loading method, the relative error was within 10%. This is reasonable because of the differences in the simulation methods. Compared with the study reported by (Zhuang et al. 2016), which simulated TP loads using DSEEM on an annual scale, the relative error was within 5%. The difference between the results can be attributed to the time variation of NDVI after improving the time resolution of the simulation. The relative error indicates the reliability of the simulation results.

(2) Load–time/area curve

The parameters of the fitting curves were presented, including the load–time curve, load–area curve in CPs, load–area curve in sub-CPs, and load–area curve in non-CPs. The R-square values of the four fitting curves were all greater than 0.94, indicating that a good fit (Table 2).

[Insert Table 2 here]

(3) CSAs after PDA

222 To evaluate the effectiveness and feasibility of the PDA, the spatial distribution and load proportion
223 of the CSAs before and after PDA were compared. The results showed that the distribution of CSAs and
224 sub-CSAs became more concentrated after PDA (Fig. 5). The area proportion of CSAs and sub-CSAs
225 increased by 36.0% and 29.9% respectively, because non-CSA grids in regions with high CSA
226 aggregation were also considered when identifying CSAs. CSAs after PDA accounted for up to 26.2%
227 of the annual load with 14.5% area, and the load/area value was 1.81, which was important for the control
228 of NPS pollution in the entire region.
229 [Insert Fig. 5 here]
230
231 **3.2 Spatiotemporal distribution characteristics of TP load**
232 The TP load in the DRB showed significant spatiotemporal heterogeneities (Fig. 6). The variation
233 and distribution of the TP load in the reservoir area are consistent with rainfall and NDVI, respectively
234 (Fig. 3 and Fig. 4 in the Appendix). The monthly total TP loads ranged from high to low in July, April,
235 September, May, March, August, June, October, February, November, December, and January. The total
236 TP load in June, October, February, November, December, and January were less than 0.02 × 10^4 t. In
237 July, the TP loads accounted for 39.2% of the entire year because of high rainfall and low vegetation
238 coverage, especially in the central part of the reservoir (Fig. 6g). Although it differed slightly from the
239 total TP loads in April, September, May, March, and August, the distribution characteristics and the main
240 factors affecting the distribution were different. In March and April with low rainfall and vegetation
241 coverage, the spatial distribution of TP loads was relatively homogeneous, especially in forest and
242 shrubland around the DRB. In May, due to the variation in NDVI, the TP load was concentrated in the
243 middle of the reservoir. During high rainfall (August and September), areas around the reservoir, which

were dominated by forest, had high vegetation coverage. Areas with high TP loads were mainly concentrated in farmland and shrubland in the middle of the reservoir, and the distribution was consistent with the slope (Fig. 2b in the Appendix). Therefore, rainfall and vegetation coverage are the most important factors that impact the seasonal distribution of TP loads.

[Insert Fig. 6 here]

3.3 Cooperative analysis of CPs and CSAs

3.3.1 Fitted curve of CPs

CPs were identified quantitatively using the fitted cumulative load–periods curve (Fig. 9a). The slope k of the fitting curve represents the increasing load rate with periods. The load changes heterogeneously as the area grows. When k was 1, 27.9% of the time contributed 70.8% of the load. Therefore, we identified July, April, and September as the CPs of the TP NPS pollution in the DRB in 2010, which contributed 62.9% of the annual TP load with a 25.0% proportion of the period. In addition, when k was 0.5, 55.8% of the time contributed 90.1% of the load. May, March, and August were identified as sub-CPs, accounting for 31.0% TP load with 25.0% proportion of the period, and the remaining months (June, October, February, November, December, and January) were identified as non-CPs, accounting for 6.1% of the TP load with 50.0% proportion of the period.

3.3.2 Fitted curve of CSAs in CPs

CSAs during the different periods (CP, sub-CP, and non-CP) were confirmed based on the TP loads and the identified CPs (Fig. 9b; 9c; 9d). The uneven increase in the k' value indicates the heterogeneity of the spatial distribution of TP loads. Compared with the load distribution in sub-CPs and non-CPs, the

load distribution in CPs was more concentrated (the slope of the fitting curve is steeper and the rate of change is faster).

Considering the spatial distribution characteristics of the TP load in the study area, the slope of the fitting curve of 2 was used as the boundary to divide the CSAs and sub-CSAs, and the slope of the fitting curve of 1 was used as the boundary to divide sub-CSAs and non-CSAs. For CPs, when k' was 2, the corresponding critical value of TP load was 2.72 kg/ha, and 10.7% of the areas contributed 31.3% of the annual TP load. When k' was 1, the corresponding critical value of TP load was 1.35kg/ha, and 21.4% of the area contributed 43.3% of the load. For sub-CSAs, when k' was 2, 11.2% of the area contributed 13.6% of the annual load, when k' was 1, 22.4% of the area contributed 18.9% of annual TP load. For non-CPs, 9.5% of the area within CSAs contributed 3.5% of the annual load, and 19.1% of the area in sub-CSAs contributed 4.6% of the annual load.

[Insert Fig. 9 here]

3.4 Spatiotemporal distribution characteristics of CSAs

The spatial distribution of CSAs varied during different periods due to the spatiotemporal changes in rainfall and vegetation coverage (Fig. 3 and Fig. 4 in the Appendix; Fig. 10). According to previous studies, Xichuan and Yunxian counties are the most polluted in the DRB (Jiang et al. 2010), which is consistent with our results. During the CPs, the CSAs were concentrated in the middle and west of the reservoir area, mainly in Xichuan and Yunxian counties (Fig. 10; Fig. 11a), contributing 20.0% of the annual TP load. During sub-CPs, in addition to Yunxian and Xichuan County, Yunxi counties, which is located in the western part of the DRB, also had a large area of CSA clusters, contributing 1.7% of the annual TP load. CSAs in non-CPs shifted toward the south and were mainly distributed in the central part

of Yunxian County and the south-central part of Yunxi County.

[Insert Fig. 10 here]

The results showed that farmland, shrubland, and forest were the main sources of phosphorus in the region, contributing up to 91.7% of the annual TP load (Fig. 11b). Of the total TP load, 62.3% originates from the CP, and 23.8% of the load originates from the CSA during the CP. Approximately 94.2% of farmland was dry land, with 42.9% located in an area with a slope of 5–15° and 18.7% with a slope greater than 15°. In the TP load contributed by farmland, 63.4% of the load was generated during CPs (mainly in July) when rainfall was high and extensive amount of fertilizer was used (Huang et al. 2012). These conditions aggravated the soil erosion of farmland and resulted in high phosphorus NPS pollution. For shrubland and forest, 63.4% and 59.1% of TP loads originated from CPs, respectively. During CPs, low vegetation coverage in these areas causes high soil erosion risk and high TP loss risk (Sun et al. 2008). In addition, the low vegetation coverage of grasslands in the central part of Xichuan County (Zhuang et al. 2016) also resulted in a high TP concentration of grassland in CPs.

[Insert Fig. 11 here]

3.5 Preferred hierarchical control strategies for NPS

Prior to causing NPS pollution, nutrients are impacted by processes such as vegetation interception, river sedimentation, and water self-purification (Frankenberger et al. 2015). Therefore, all NPS sources do not need to be controlled effectively. Periods and areas that generate disproportionately high pollutant loads, were prioritized using the cooperative analysis of CPs and CSAs. For this, a preferred hierarchical control strategy was proposed to achieve efficient short-term and small-scale prevention and control of NPS pollution. Three levels were classified according to the concentration of TP loads: class I (CSAs in

CPs) → class II (sub-CSAs in CPs, CSAs in sub-CPs) → class III (non-CPs, non-CSAs, sub- and non-CSAs in sub-CPs) (Table 3).

[Insert Table 3 here]

Class I (CSA in CP) contributed 26.2% of the annual load, accounting for 14.5% of the area and 25.0% of the time. The farmland distributed in the slope fields of the central and northeastern parts of Yunxian County and the northern part of Xichuan County are the main sources of phosphorus NPS pollution. The poor retention and water conservation capacity of dryland (Fu et al. 2006) combined with the impact of intense rainfall, steep slopes, and fertilizer overuse (Huang et al. 2012), caused the high soil loss risk of farmland during this period. For slope farmland under the eco-compensation policy, measures can be taken to return farmland to forest and grassland to reduce runoff and control soil erosion (Tang et al. 2011). Hedgerows can be constructed in farmland with a relatively gentle slope. In addition, replacing traditional fertilization with slow-controlled fertilization and combined application of organic and inorganic fertilizers (Liu et al. 2016a) can greatly reduce the loss of fertilizer at the early stage of crop growth. In addition to shrubland and forest, the grassland distribution in the central part of Xichuan County contributed a high proportion of the load. Planting grass can be considered to enhance vegetation interception.

Class II (sub-CSA in CP, CSA in sub-CP) contributed 24.0% of the TP load within 24.8% of the area and 50.0% of the time, with sub-CSA in CP contributing 13.1% of the TP load within 13.9% of the area and 25.0% of the time and CSA in sub-CP contributing 10.9% of the TP load within 14.1% of the area and 25.0% of the time. Slope farmland is also the land-use area that needs critical control, mainly distributed in the central and central and northeastern parts of Yunxian County, the central part of Xichuan County, midwest of Yunxi County, and the northern part of Danjiangkou City. Because most of these

areas are close to the water bodies, a vegetation buffer zone can be constructed. Furthermore, because agriculture is the most important pollution source in the hydro-fluctuation belt of DRB, and agricultural irrigation affects water quality, water-saving irrigation measures can be taken to mitigate phosphorus loss (Pan et al. 2020, Zhuang et al. 2019). Shrubland and forest generated 10.0% of the annual TP load during this period when rainfall decreased significantly, and NDVI was the main factor affecting CSA distribution (Fig. 4d, e, and i in the Appendix). CSAs are distributed more discretely in the shrubland and forest areas in the western, central, and southern parts of the reservoir. In these areas, planting shrubs or trees of different types and different phenological cycles can be considered to improve the stability of the ecosystem.

Class III (non-CP, non-CSA, sub- and non-CSA in sub-CP) contributed 49.8% of the TP load within 100.0% of the area and 100.0% of the time. The distribution of this part of the load shows extremely high spatiotemporal discreteness. Due to the self-purification ability (Cook et al. 2020, He et al. 2020) of the water bodies, extensive human and material resources are not required to control this pollutant load.

4 Conclusions

In this study, based on the cooperative analysis of CPs and CSAs and the PDA, a preferred hierarchical control strategy of NPS pollution connected with management units was proposed in the DRB: class I (CSAs in CPs) → class II (sub-CSAs in CPs, CSAs in sub-CPs) → class III (non-CPs, non-CSAs, sub- and non-CSAs in sub-CPs). The results showed that class I covered the periods and areas with the highest NPS pollution loads, contributed 26.2% of the annual TP load within 25.0% of the time and 14.5% of the area. The farmland distributed in the slope fields of the central and northeastern parts of Yunxian County and the northern part of Xichuan County were the main sources of phosphorus NPS pollution. Conversion

of farmland to forest, hedgerow, and reasonable fertilization regimes were advocated to mitigate NPS pollution; class II contributed 24.0% of the TP load within 24.8% of the area and 50.0% of the time, with sub-CSA in CP contributing 13.1% of the TP load within 13.9% of the area and 25.0% of the time and CSA in sub-CP contributing 10.9% of the TP load within 14.1% of the area and 25.0% of the time. Considering that most CSAs are distributed on slope farmland near water bodies, a vegetation buffer zone could be constructed; class III contributed 49.8% of the TP load within 100.0% of the area and 100.0% of the time. Extensive human and material resources were not required to control this pollutant load. This study provides a reference for the targeted control of NPS pollution at regional scale, especially in environmental protection with limited funds.

Declarations

Ethics approval and consent to participate: Not applicable.

Consent for publication: Not applicable.

Availability of data and materials: The datasets generated and/or analyzed during the current study are available in the repositories: China Soil Scientific Database (http://www.soil.csdb.cn/); Geospatial Data Cloud (http://www.gscloud.cn); Landsat 7 ETM Data (https://earthexplorer.usgs.gov/); China Meteorology Data Service Center (http://data.cma.cn).

Competing interests: The authors declare that they have no competing interests.

Funding: This work was supported by the Strategic Priority Research Program of the Chinese Academy of Sciences [No. XDA23040403], the Hubei Technological Innovation Special Fund of China [Nos. 2018ACA148 and 2019ACA155], and the Youth Innovation Promotion Association, CAS [No. 2018370].

Authors' contributions: Conceptualization: Yanhua Zhuang; Methodology: Yanhua Zhuang, Weijia Wen; Formal analysis and investigation: Yanhua Zhuang; Writing - original draft preparation: Weijia Wen; Writing - review and editing: Yanhua Zhuang, Liang Zhang, Sisi Li, Shuhe Ruan; Funding acquisition: Yanhua Zhuang, Liang Zhang; Resources: Weijia Wen, Shuhe Ruan, Qinjing Zhang; Supervision: Yanhua Zhuang.

References

Bannerman RT, Owens DW, Dodds RB, Hornewer NJ (1993) Sources of pollutants in Wisconsin stormwater. Water Sci Technol 28: 241-259. doi: 10.3321/j.issn:0253-2468.2002.04.012

Chen P, Li L, Zhang HB (2015) Spatio-temporal variations and source apportionment of water pollution in Danjiangkou Reservoir Basin, central China. Water 7: 2591-2611. doi: 10.3390/w7062591

Cook S, Price O, King A, Finnegan C, Bending GD (2020) Bedform characteristics and biofilm community development interact to modify hyporheic exchange. Sci Total Environ 749: 141397. doi: 10.1016/j.scitotenv.2020.141397

Ding XW, Shen ZY, Hong Q, Yang ZF, Wu X, Liu RM (2010) Development and test of the Export Coefficient Model in the Upper Reach of the Yangtze River. J Hydrol 383: 233-244. doi: 10.1016/j.jhydrol.2009.12.039

Drewry JJ, Newham LH, Greene RSB (2011) Index models to evaluate the risk of phosphorus and nitrogen loss at catchment scales. J Environ Manage 92: 639-649. doi: 10.1016/j.jenvman.2010.10.001

Frankenberger JR, Brooks ES, Walter MT, Walter MF, Steenhuis TS (2015) A GIS-based variable source area hydrology model. Hydrol Process 13: 805-822. doi: 10.1002/(sici)1099-1085(19990430)13:6%3c805::aid-hyp754%3e3.0.co;2-m

Fu GB, Chen SL, McCool DK (2006) Modeling the impacts of no-till practice on soil erosion and sediment yield with RUSLE, SEDD, and ArcView GIS. Soil Tillage Res 85: 38-49. doi: 10.1016/j.still.2004.11.009

Gburek WJ, Sharpley AN (1998) Hydrologic controls on phosphorus loss from upland agricultural watersheds. J Environ Qual 27: 267-277. doi: 10.2134/jeq1998.00472425002700020005x

Ghebremichael LT, Veith TL, Hamlett JM (2013) Integrated watershed- and farm-scale modeling

framework for targeting critical source areas while maintaining farm economic viability. Journal of environmental management 114: 381-94. doi: 10.1016/j.jenvman.2012.10.034

Hao FH, Zhang XS, Yang ZF (2004) A distributed non-point source pollution model: Calibration and validation in the Yellow River Basin. J Environ Sci 16: 646-650. doi: 10.3321/j.issn:1001-0742.2004.04.025

He X, Chen G, Fang Z, Liang W, Li B, Tang J, Sun Y, Qin L (2020) Source identification of chromium in the sediments of the Xiaoqing River and Laizhou Bay: A chromium stable isotope perspective. Environ Pollut 264: 114686. doi: 10.1016/j.envpol.2020.114686

Huang Q, Huang J, Yang X, Ren L, Tang C, Zhao L (2017) Evaluating the scale effect of soil erosion using landscape pattern metrics and information entropy: a case study in the Danjiangkou reservoir area, China. Sustainability 9: 1243. doi: 10.3390/su9071243

Huang W, Bi Y, Hu Z, Wang H, Feng R, Hu J (2012) Study on characteristics of agricultural non-point source pollution in Danjiangkou Reservoir. Environ Sci Manage (China) 37: 33-38. doi: 10.3969/j.issn.1673-1212.2012.01.008

Jiang Q, Zhou P, Liao C, Liu Y, Liu F (2020) Spatial pattern of soil erodibility factor (K) as affected by ecological restoration in a typical degraded watershed of central China. Sci Total Environ 749: 141609. doi: 10.1016/j.scitotenv.2020.141609

Jiang S, Han P, Jia Z, Mao X, Si J, Ye F (2010) Evaluation with PSR Model and GIS Analysis of Agricultural Non-point Source Pollution in Danjiangkou Reservoir of the Mid-Route of the South-to-North Water Transfer Project. J Agro-Environ Sci (China) 29: 2153-2162. doi:

Johnes PJ (1996) Evaluation and management of the impact of land use change on the nitrogen and phosphorus load delivered to surface waters: The export coefficient modelling approach. J Hydrol 183: 323-349. doi: Doi 10.1016/0022-1694(95)02951-6

Kaplowitz MD, Lupi F (2012) Stakeholder preferences for best management practices for non-point source pollution and stormwater control. Landsc Urban Plan 104: 364-372. doi: 10.1016/j.landurbplan.2011.11.013

Le C, Zha Y, Li Y, Sun D, Lu H, Yin B (2010) Eutrophication of lake waters in China: cost, causes, and control. Environ Manage 45: 662-8. doi: 10.1007/s00267-010-9440-3

Lemunyon JL, Gilbert RG (1993) The concept and need for a phosphorus assessment-tool. J Prod Agric 6: 483-486. doi: Doi 10.2134/Jpa1993.0483

Li S, Gitau M, Bosch D, Engel BA, Zhang L, Du Y (2017) Development of a soil moisture-based distributed hydrologic model for determining hydrologically based critical source areas. Hydrol Process 31: 3543-3557. doi: 10.1002/hyp.11276

Liu RH, Kang YH, Wan SQ, Pei L (2016a) Evaluation of methods of nutrient and water management on tea performance and nutrient loss in the Danjiangkou Reservoir area, China. Arch Agron Soil Sci 62: 1123-1135. doi: 10.1080/03650340.2015.1115017

Liu RM, Xu F, Zhang PP, Yu WW, Men C (2016b) Identifying non-point source critical source areas based on multi-factors at a basin scale with SWAT. J Hydrol 533: 379-388. doi: 10.1016/j.jhydrol.2015.12.024

Nelson NO, Shober AL (2012) Evaluation of phosphorus indices after twenty years of science and development. J Environ Qual 41: 1703-10. doi: 10.2134/jeq2012.0342

Niraula R, Kalin L, Srivastava P, Anderson CJ (2013) Identifying critical source areas of nonpoint source pollution with SWAT and GWLF. Ecol Model 268: 123-133. doi: 10.1016/j.ecolmodel.2013.08.007

Nong X, Shao D, Zhong H, Liang J (2020) Evaluation of water quality in the South-to-North Water Diversion Project of China using the water quality index (WQI) method. Water Res 178: 115781. doi: 10.1016/j.watres.2020.115781

Ongley ED, Xiaolan Z, Tao Y (2010) Current status of agricultural and rural non-point source Pollution assessment in China. Environ Pollut 158: 1159-68. doi: 10.1016/j.envpol.2009.10.047

Pan L, Han Y, Wang H (2020) Spatial–temporal variation of nitrogen and diffusion flux across the water–sediment interface at the hydro-fluctuation belt of Danjiangkou reservoir in China. Water Sup 20: 1241-1252. doi: 10.2166/ws.2020.044

Panagopoulos Y, Makropoulos C, Baltas E, Mimikou M (2011) SWAT parameterization for the identification of critical diffuse pollution source areas under data limitations. Ecol Model 222: 3500-3512. doi: 10.1016/j.ecolmodel.2011.08.008

Pradhanang SM, Briggs RD (2014) Effects of critical source area on sediment yield and streamflow. Water Environ J 28: 222-232. doi: 10.1111/wej.12028

Ruan S, Zhuang Y, Hong S, Zhang L, Wang Z, Tang X, Wen W (2020) Cooperative identification for critical periods and critical source areas of nonpoint source pollution in a typical watershed in China. Environ Sci Pollut Res 27: 10472-10483. doi: 10.1007/s11356-020-07630-w

Sharpley AN, Daniel TC, Edwards DR (1993) Phosphorus movement in the landscape. J Prod Agric 6: 492-500. doi: 10.2134/Jpa1993.0492

Sharpley AN, Weld JL, Beegle DB, Kleinman PJA, Gburek WJ, Moore PA, Mullins G (2003) Development of phosphorus indices for nutrient management planning strategies in the United States. J Soil Water Conserv 58: 137-152.

Shen H, Zhang W, Peng H (2010) Research on soil erosion and particulate phosphorus load of non-point source pollution in the middle and lower reaches of the Hanjiang River basin. Res Soil Water Conserv (China) 17: 1-6.

Shen W, Zhang L, Li S, Zhuang Y, Liu H, Pan J (2020) A framework for evaluating county-level non-point source pollution: Joint use of monitoring and model assessment. Sci Total Environ 722: 137956. doi: 10.1016/j.scitotenv.2020.137956

Shi Z, Cai C, Ding S, LI Z, Wang T, Zhang B, Shen X (2002) Research on nitrogen and phosphorus load of agricultural non-point sources in middle and lower reaches of Hanjiang River besed on GIS. Acta Sci Circumst (China) 22: 473-477.

Shrestha NK, Rudra RP, Daggupati P, Goel PK, Shukla R (2021) A comparative evaluation of the continuous and event-based modelling approaches for identifying critical source areas for sediment and phosphorus losses. J Environ Manage 277: 111427. doi: 10.1016/j.jenvman.2020.111427

Soranno PA, Hubler SL, Carpenter SR, Lathrop RC (1996) Phosphorus loads to surface waters: A simple model to account for spatial pattern of land use. Ecol Appl 6: 865-878. doi: 10.2307/2269490

Sun ZC, Shi ZH, Ng SL, Li L, Li Z, Cai CF (2008): Mapping soil erosion risk in Danjiangkou Reservoir area using RUSLE, RS and GIS: a case study of Danjiangkou City, International Conference on Informational Technology & Environmental

Tang LH, Yang DW, Hu HP, Gao B (2011) Detecting the effect of land-use change on streamflow, sediment and nutrient losses by distributed hydrological simulation. J Hydrol 409: 172-182. doi: 10.1016/j.jhydrol.2011.08.015

Tian Y, Huang Z, Xiao W (2010) Reductions in non-point source pollution through different management practices for an agricultural watershed in the Three Gorges Reservoir Area. J Environ Sci: 184-

191. doi: 10.1016/S1001-0742(09)60091-7

Vander Zanden M, Vadeboncoeur Y, Diebel M, Jeppesen E (2005) Primary consumer stable nitrogen isotones as indicators of nutrient source. Environ Sci Technol 39: 7509-7515. doi: 10.1021/es050606t

Wang W, Chen L, Shen Z (2020) Dynamic export coefficient model for evaluating the effects of environmental changes on non-point source pollution. Sci Total Environ 747: 141164. doi: 10.1016/j.scitotenv.2020.141164

Wang X, Wang Q, Wu C, Liang T, Zheng D, Wei X (2012) A method coupled with remote sensing data to evaluate non-point source pollution in the Xin'anjiang catchment of China. Sci Total Environ 430. doi: 10.1016/j.scitotenv.2012.04.052

Wang Y, Yang J, Liang J, Qiang Y, Fang S, Gao M, Fan X, Yang G, Zhang B, Feng Y (2018) Analysis of the environmental behavior of farmers for non-point source pollution control and management in a water source protection area in China. Sci Total Environ 633: 1126-1135. doi: 10.1016/j.scitotenv.2018.03.273

Xue L, Hou P, Zhang Z, Shen M, Liu F, Yang L (2020) Application of systematic strategy for agricultural non-point source pollution control in Yangtze River basin, China. Agric Ecosyst Environ 304: 107148. doi: 10.1016/j.agee.2020.107148

Yu H, Xi B, Jiang J, Heaphy MJ, Wang H, Li D (2011) Environmental heterogeneity analysis, assessment of trophic state and source identification in Chaohu Lake, China. Environ Sci Pollut Res 18: 1333-42. doi: 10.1007/s11356-011-0490-8

Zhang Z, Huang P, Chen ZH, Li JM (2019) Evaluation of distribution properties of non-point source pollution in a subtropical monsoon watershed by a hydrological model with a modified runoff module. Water 11: 993. doi: Artn 99310.3390/W11050993

Zhuang YH, Zhang L, Du Y, Yang WJ, Wang LH, Cai XB (2016) Identification of critical source areas for nonpoint source pollution in the Danjiangkou Reservoir Basin, China. Lake Reserv Manage 32: 341-352. doi: 10.1080/10402381.2016.1204396

Zhuang YH, Zhang L, Li SS, Liu HB, Zhai LM, Zhou F, Ye YS, Ruan SH, Wen WJ (2019) Effects and potential of water-saving irrigation for rice production in China. Agr Water Manage 217: 374-382. doi: 10.1016/j.agwat.2019.03.010

Table captions

Table 1 Environmental data of DRB

Table 2 Fit and accuracy of cumulative load–time curve and cumulative load–area curve

Table 3 Load and area contribution of different periods and areas and classification of NPS pollution control

Figure captions

Fig. 1 Location of the DRB: (a) location of the DRB as seen on the Chinese map; (b) location of the DRB in the Yangtze River Basin; and (c) elevation of the DRB

Fig. 2 Spatial distribution of soil erosion in DRB: (a) land-use; (b) slope degree (in the Appendix)

Fig. 3 Monthly rainfall of the 10 weather stations near DRB in 2010 (in the Appendix)

Fig. 4 NDVI of DRB: (a) to (l) represent January to December (in the Appendix)

Fig. 5 Comparison of CSA distribution in CPs before and after PDA: (a) before PDA and (b) after PDA

Fig. 6 Distribution of unit TP load (kg/ha) in DRB in 2010: (a) to (l) represent January to December

Fig. 7 Distribution of unit particulate phosphorus (PP) load (kg/ha) in DRB in 2010: (a) to (l) represent January to December (in the Appendix)

Fig. 8 Distribution of unit dissolved phosphorus (DP) load (kg/ha) in DRB in 2010: (a) to (l) represent January to December (in the Appendix)

Fig. 9 Cumulative load–time fitting curve (a) and cumulative load–area fitting curves (b–d): (a) cumulative load–time curve; (b) cumulative load–area curve of CSAs in CPs; (c) cumulative load–area curve of CSAs in sub-CPs; and (d) cumulative load–area curve of CSAs in non-CPs

Fig.10 Spatial distribution of CSAs during different periods: (a) in CPs; (b) in sub-CPs; and (c) in non-CPs

550 **Fig. 11** Proportion of TP loads in different periods and areas: (a) within each county and (b) within each

551 land-use type

552

553 **Table 1** Environmental data of DRB

Database	Format	Description	Source
Soil type	Vector	1:400, 000 Chinese soil distribution vector map	China Soil Scientific Database, Institute of Soil Science, Chinese Academy of Sciences (CAS)(http://www.soil.csdb.cn/)
DEM	Raster	30M resolution digital elevation data	Geospatial Data Cloud (http://www.gscloud.cn)
Land-use	Raster	Including forest, grassland, farmland, shrubland, wasteland, construction land, orchard and wetland	Interpreted from Landsat 7 ETM data (https://earthexplorer.usgs.gov/)
NDVI	Raster	Monthly data set, calculated by MODND1D	Geospatial Data Cloud (http://www.gscloud.cn/)
Rainfall	Excel	Daily rainfall data set (1991~ 2010) of 10 weather stations	China Meteorology Data Service Center (http://data.cma.cn）

554

555

556 **Table 2** Fit and accuracy of cumulative load–time curve and cumulative load–area curve

Description	a		b		Statistics
	Value	S.E.	Value	S.E.	R^2
Load–time curve	27.923	1.895	−22.187	7.305	0.952
Load–area curve in CPs	21.356	0.003	3.910	0.010	0.971
Load–area curve in sub-CPs	22.430	0.004	−4.268	0.013	0.953
Load–area curve in non-CPs	19.052	0.003	17.510	0.010	0.962

557 fitting function: $y = a \times \ln(x) + b$

Table 3 Load and area contribution of different periods and areas and classification of NPS pollution control

Descriptions	Month	Region	Load ($\times 10^4$ t)	Load (%)	Area (%)	Class
		CSA	0.080	26.2	14.5	I
CP	7, 4, 9	sub-CSA	0.040	13.1	13.9	II
		non-CSA	0.071	23.5	71.6	III
sum	**-**	**-**	**0.191**	**62.8**	**100.0**	**-**
		CSA	0.033	10.9	14.1	II
sub-CP	5, 3, 8	sub-CSA	0.023	7.5	18.5	III
		non-CSA	0.038	12.7	67.4	III
sum	**-**	**-**	**0.094**	**31.1**	**100.0**	**-**
	6, 10,	CSA	0.008	2.8	13.5	III
non-CP	2, 11,	sub-CSA	0.005	1.5	13.8	III
	12, 1	non-CSA	0.006	1.8	72.7	III
sum	**-**	**-**	**0.019**	**6.1**	**100.0**	**-**

Class is the NPS pollution control level.

562 **Fig. 1** Location of the DRB: (a) l location of the DRB as seen on the Chinese map; (b) location of the

563 DRB in the Yangtze River Basin; and (c) elevation of the DRB

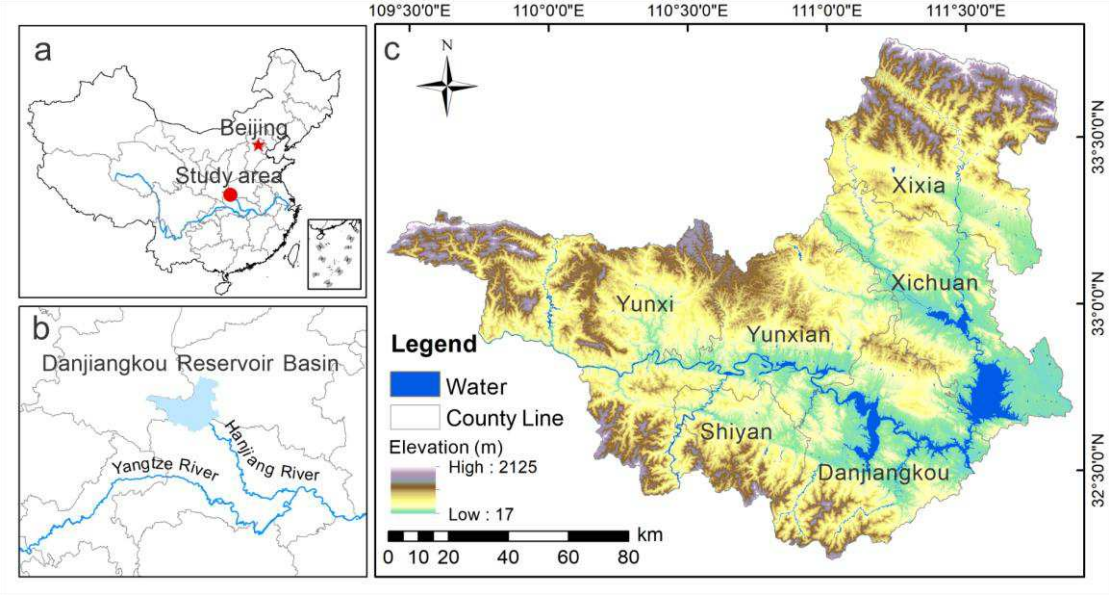

564

565 **Fig. 5** Comparison of CSA distribution in CPs before and after PDA: (a) before PDA and (b) after PDA

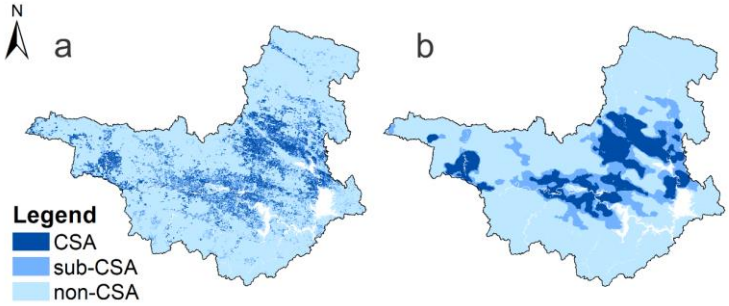

566

Fig. 6 Distribution of TP load in DRB: (a) to (l) represent January to December

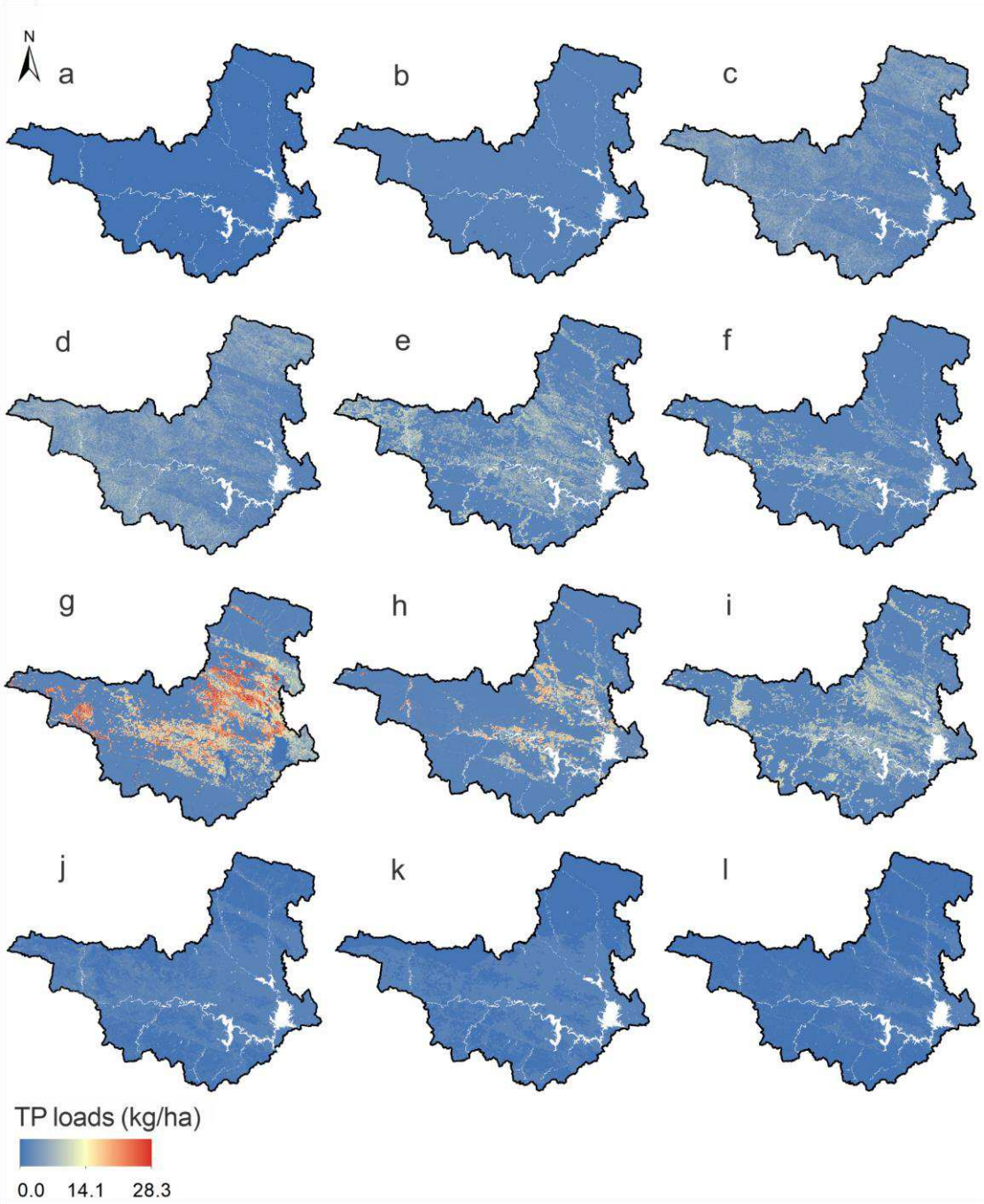

Fig. 9 Cumulative load–time fitting curve (a) and cumulative load–area fitting curves (b–d): (a) cumulative load–time curve; (b) cumulative load–area curve of CSAs in CPs; (c) cumulative load–area curve of CSAs in sub-CPs; and (d) cumulative load–area curve of CSAs in non-CPs

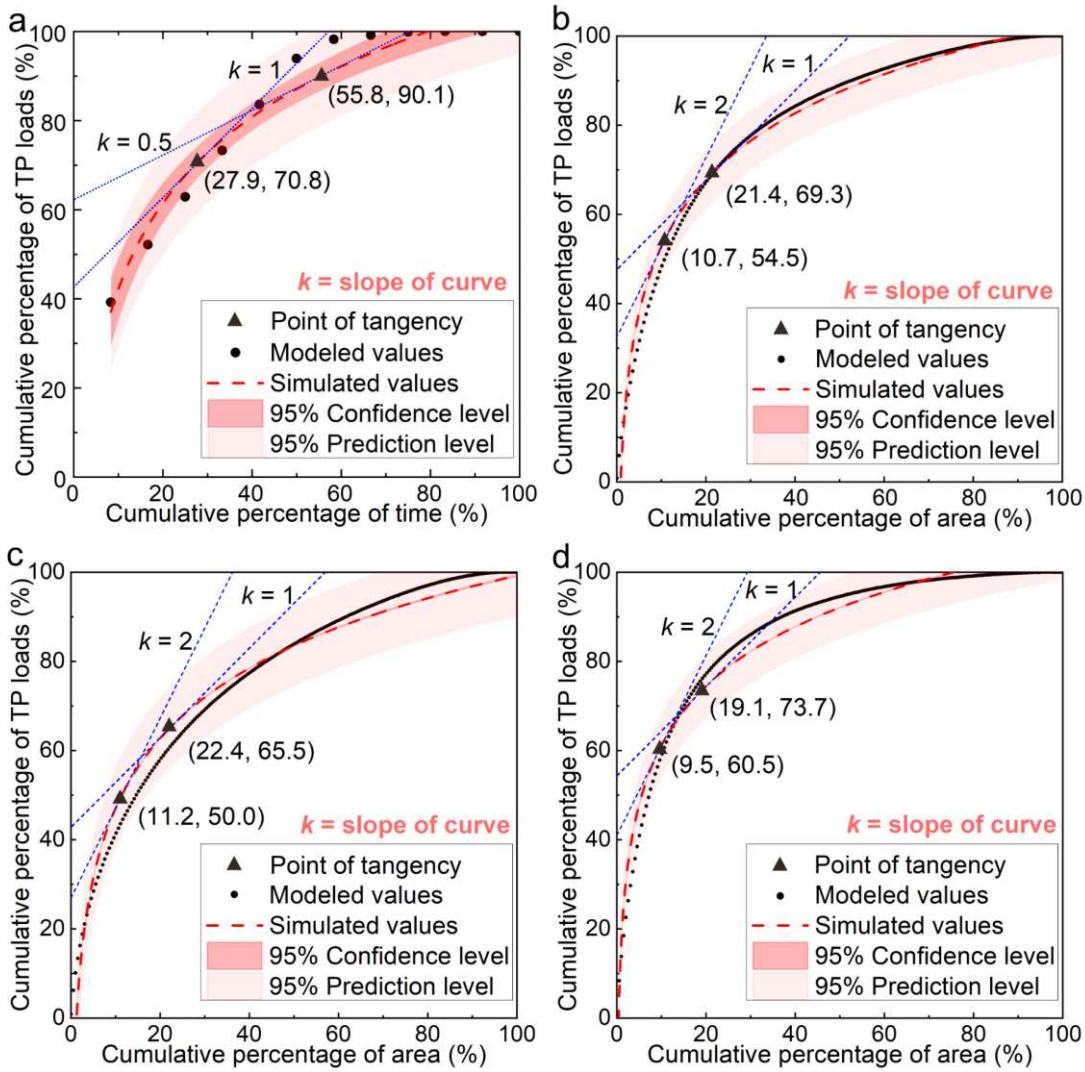

572 **Fig. 10** Spatial distribution of CSAs during different periods: (a) in CPs; (b) in sub-CPs; and (c) in non-

573 CPs

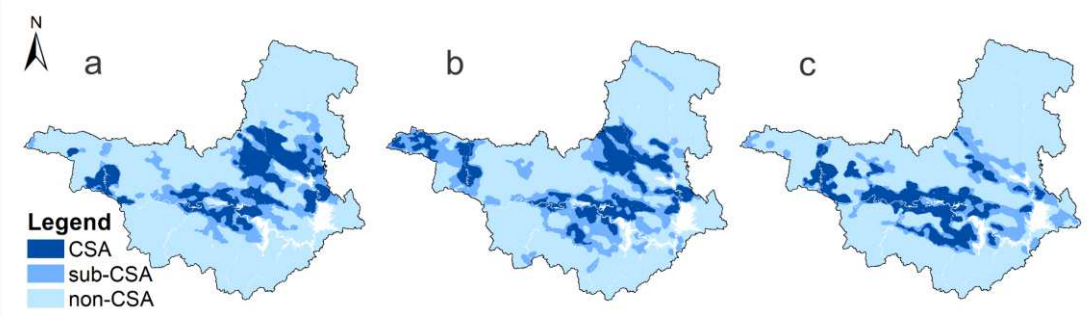

574

575 **Fig. 11** Proportion of TP loads in different periods and areas: (a) within each county and (b) within each

576 land-use type

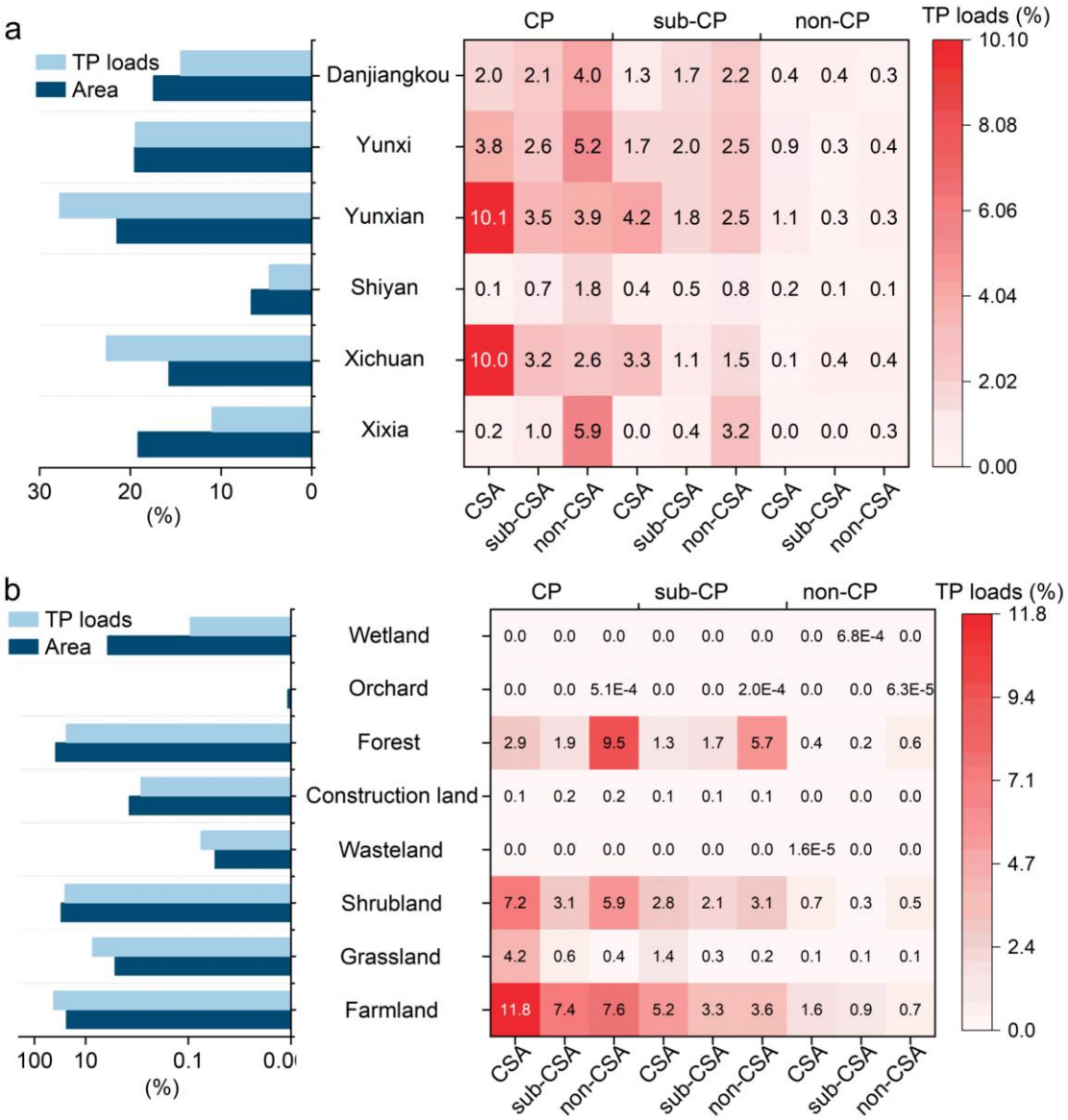

Figures

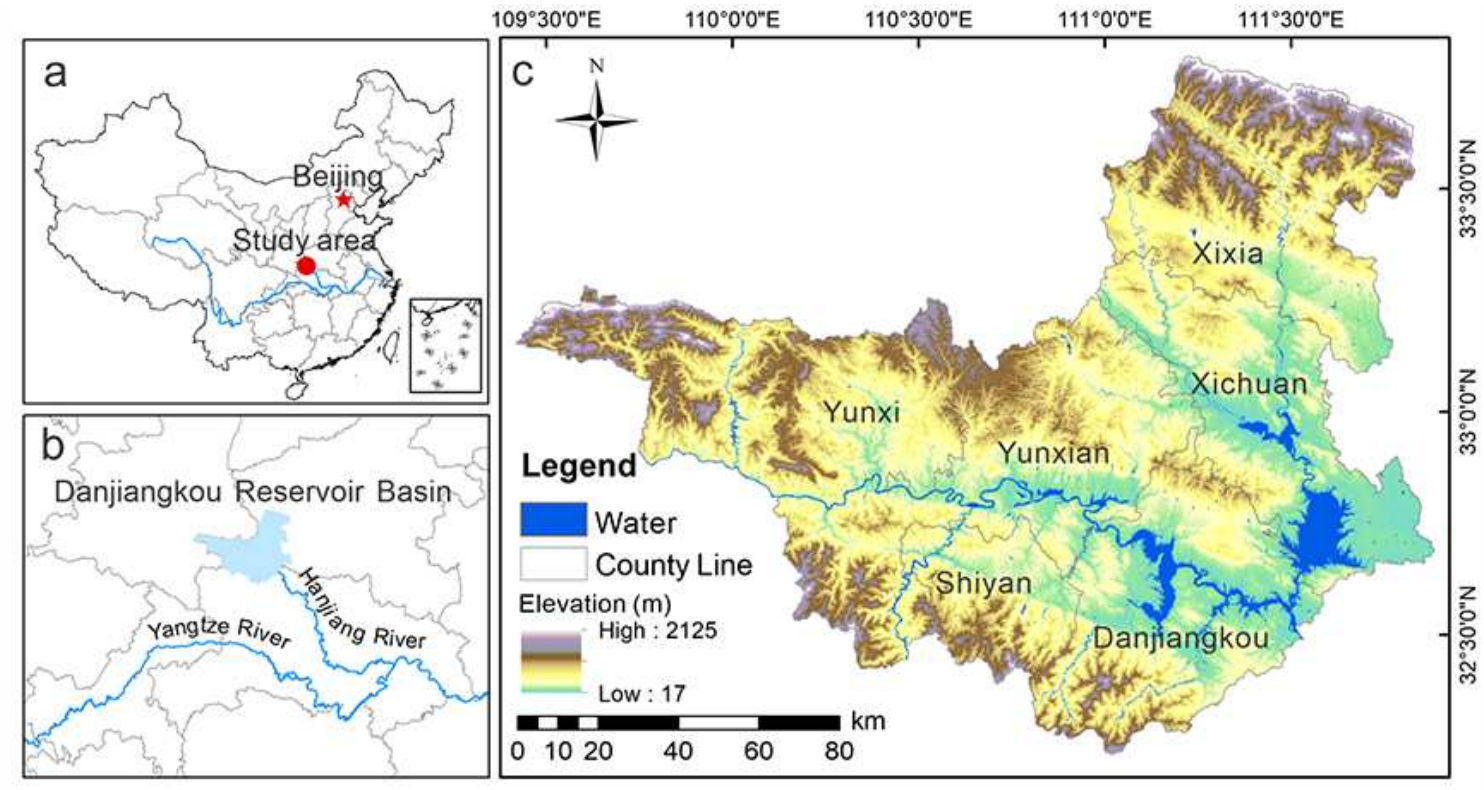

Figure 1

Location of the DRB: (a) location of the DRB as seen on the Chinese map; (b) location of the DRB in the Yangtze River Basin; and (c) elevation of the DRB Note: The designations employed and the presentation of the material on this map do not imply the expression of any opinion whatsoever on the part of Research Square concerning the legal status of any country, territory, city or area or of its authorities, or concerning the delimitation of its frontiers or boundaries. This map has been provided by the authors.

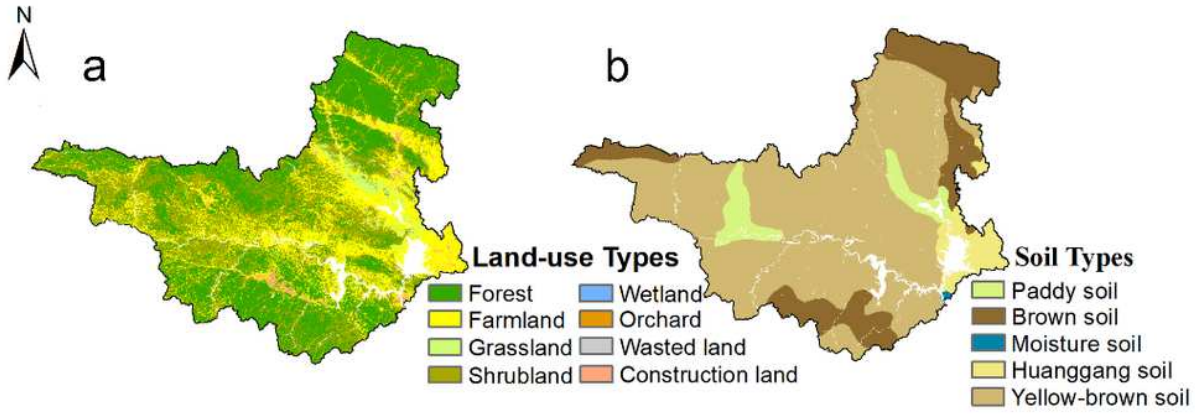

Figure 2

Spatial distribution of soil erosion in DRB: (a) land-use; (b) slope degree (in the Appendix) Note: The designations employed and the presentation of the material on this map do not imply the expression of

any opinion whatsoever on the part of Research Square concerning the legal status of any country, territory, city or area or of its authorities, or concerning the delimitation of its frontiers or boundaries. This map has been provided by the authors.

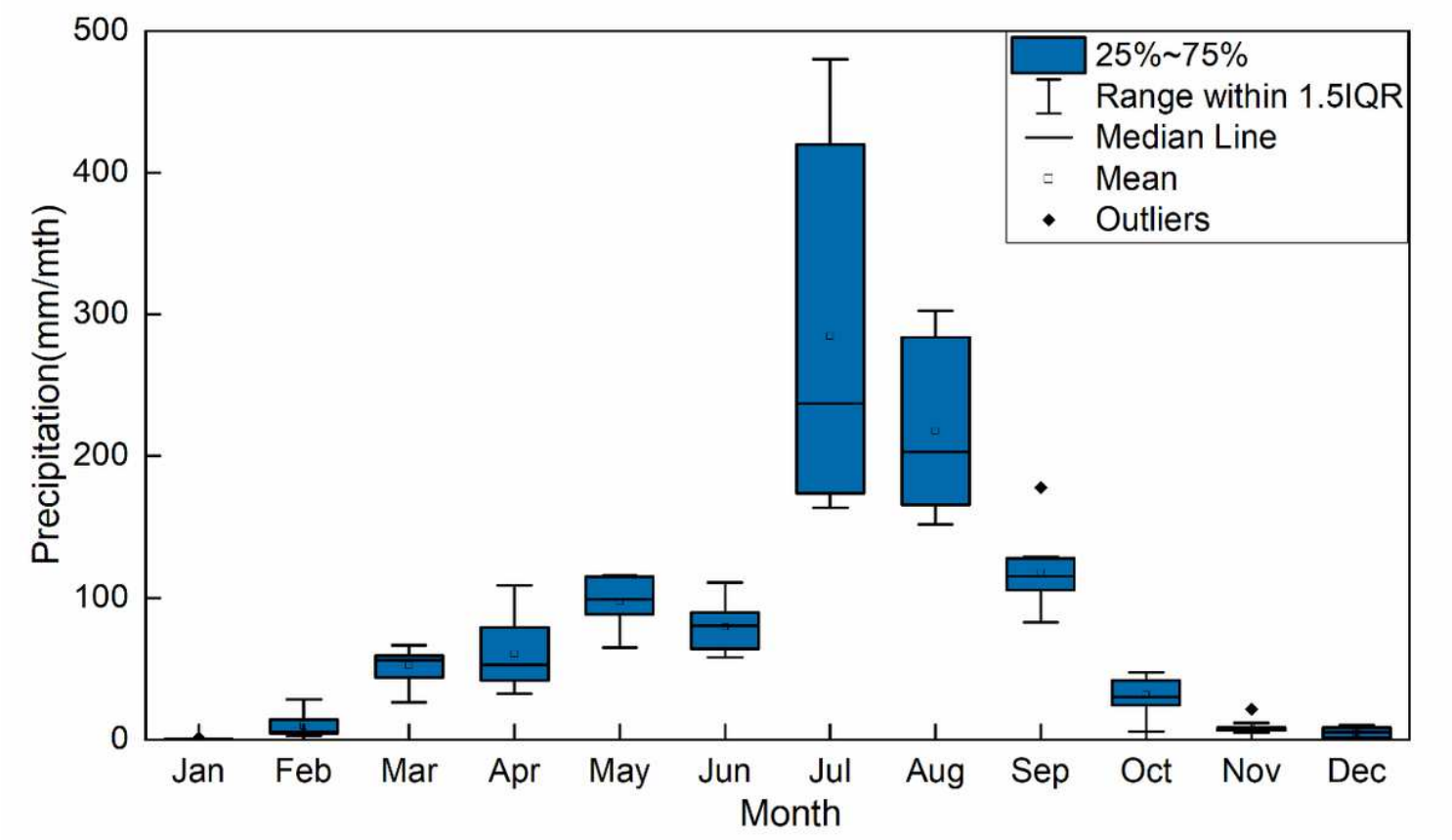

Figure 3

Monthly rainfall of the 10 weather stations near DRB in 2010 (in the Appendix)

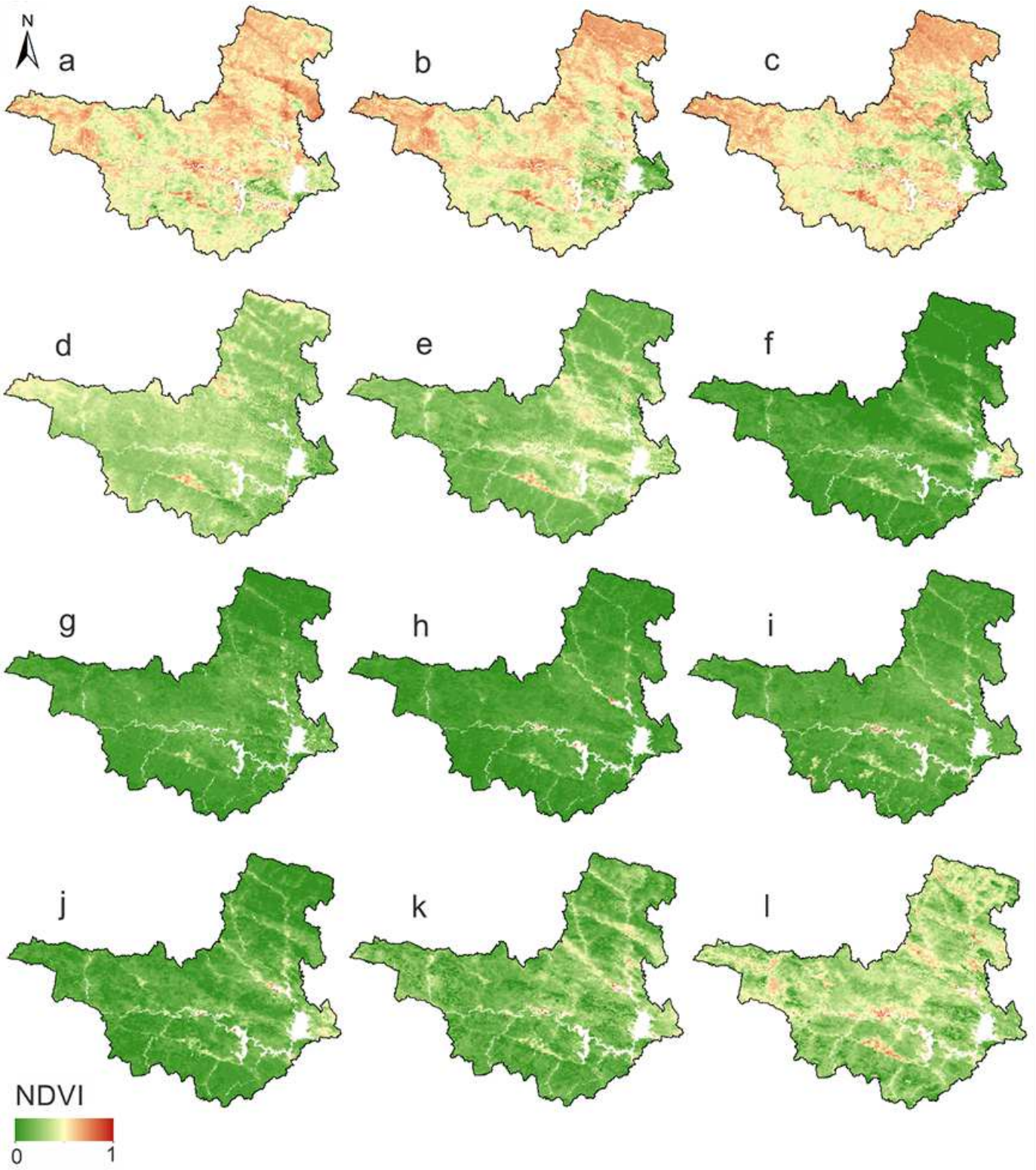

Figure 4

NDVI of DRB: (a) to (l) represent January to December (in the Appendix) Note: The designations employed and the presentation of the material on this map do not imply the expression of any opinion whatsoever on the part of Research Square concerning the legal status of any country, territory, city or area or of its authorities, or concerning the delimitation of its frontiers or boundaries. This map has been provided by the authors.

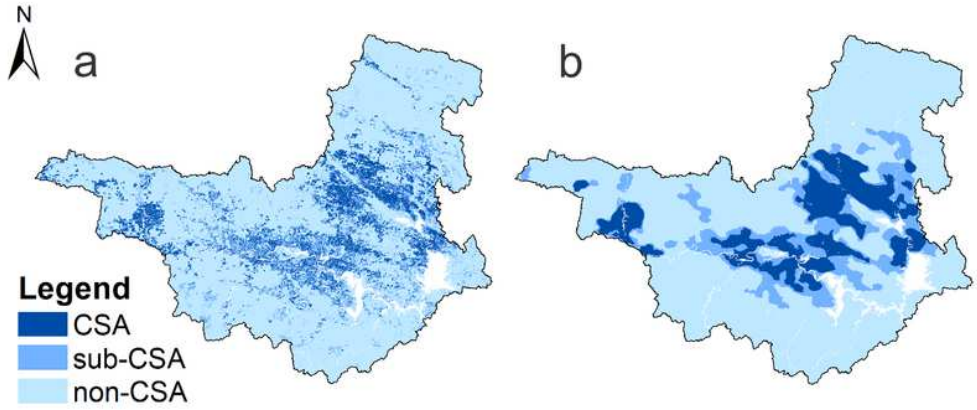

Figure 5

Comparison of CSA distribution in CPs before and after PDA: (a) before PDA and (b) after PDA Note: The designations employed and the presentation of the material on this map do not imply the expression of any opinion whatsoever on the part of Research Square concerning the legal status of any country, territory, city or area or of its authorities, or concerning the delimitation of its frontiers or boundaries. This map has been provided by the authors.

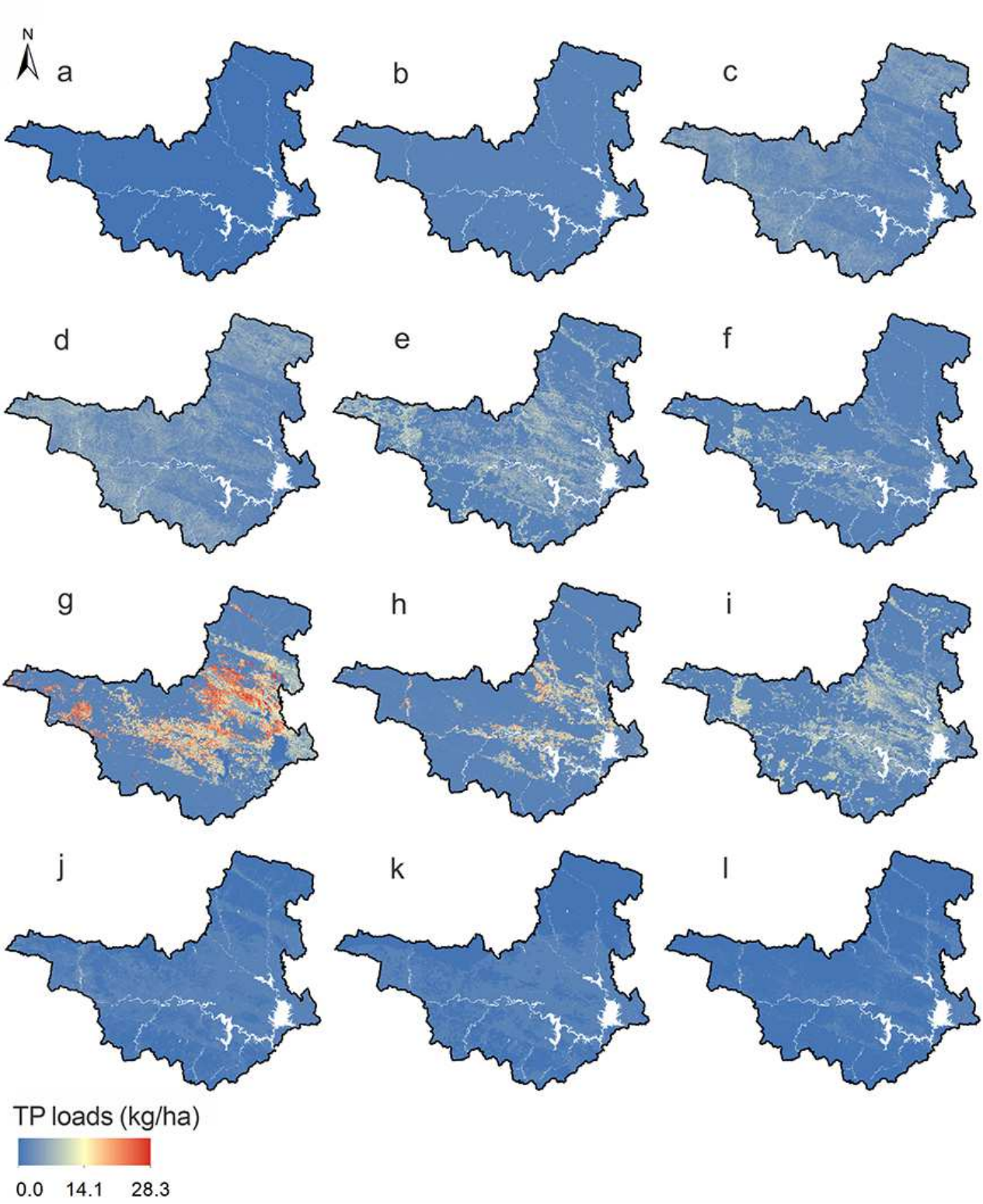

Figure 6

Distribution of unit TP load (kg/ha) in DRB in 2010: (a) to (l) represent January to December Note: The designations employed and the presentation of the material on this map do not imply the expression of any opinion whatsoever on the part of Research Square concerning the legal status of any country, territory, city or area or of its authorities, or concerning the delimitation of its frontiers or boundaries. This map has been provided by the authors.

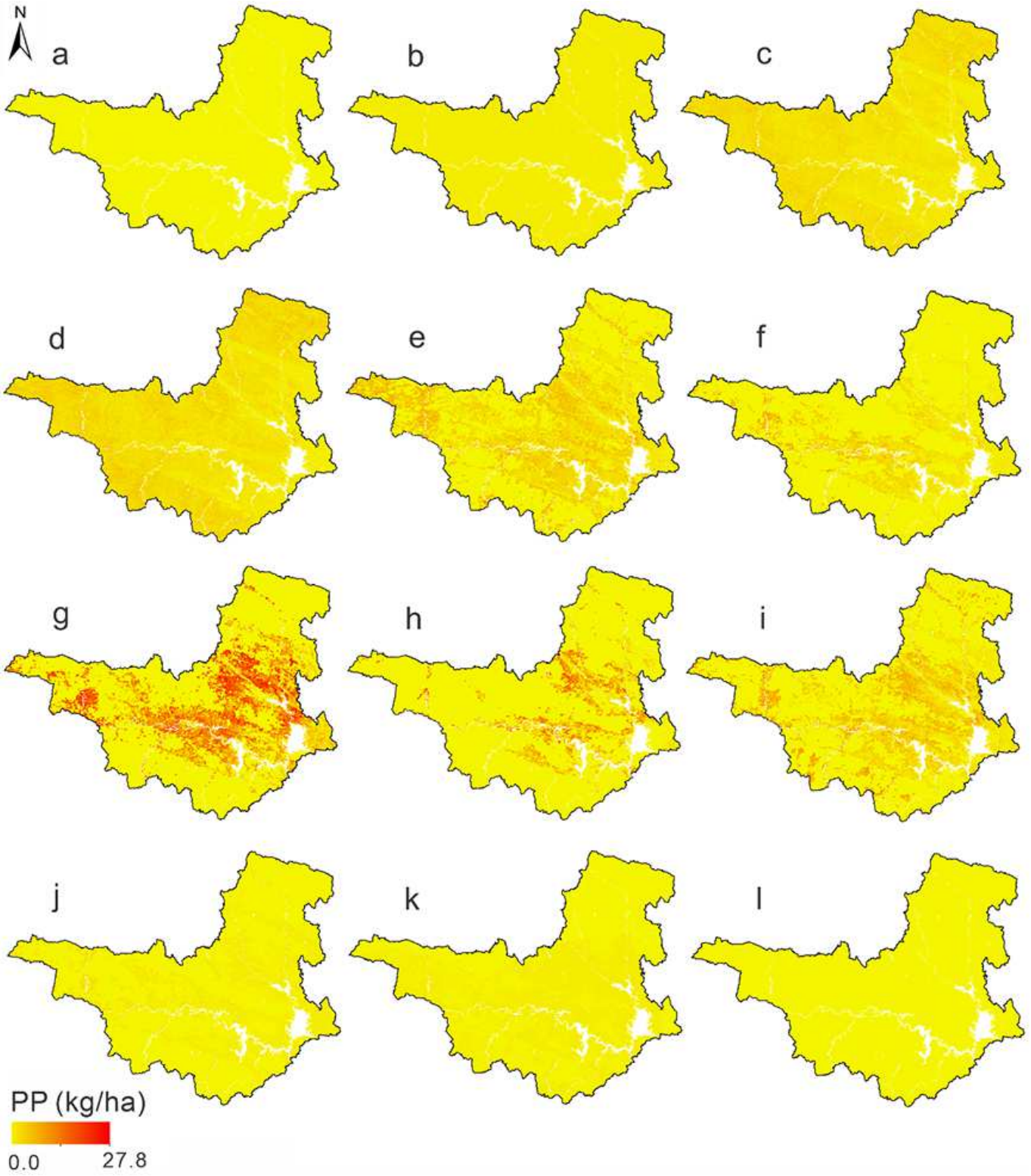

Figure 7

Distribution of unit particulate phosphorus (PP) load (kg/ha) in DRB in 2010: (a) to (l) represent January to December (in the Appendix) Note: The designations employed and the presentation of the material on this map do not imply the expression of any opinion whatsoever on the part of Research Square concerning the legal status of any country, territory, city or area or of its authorities, or concerning the delimitation of its frontiers or boundaries. This map has been provided by the authors.

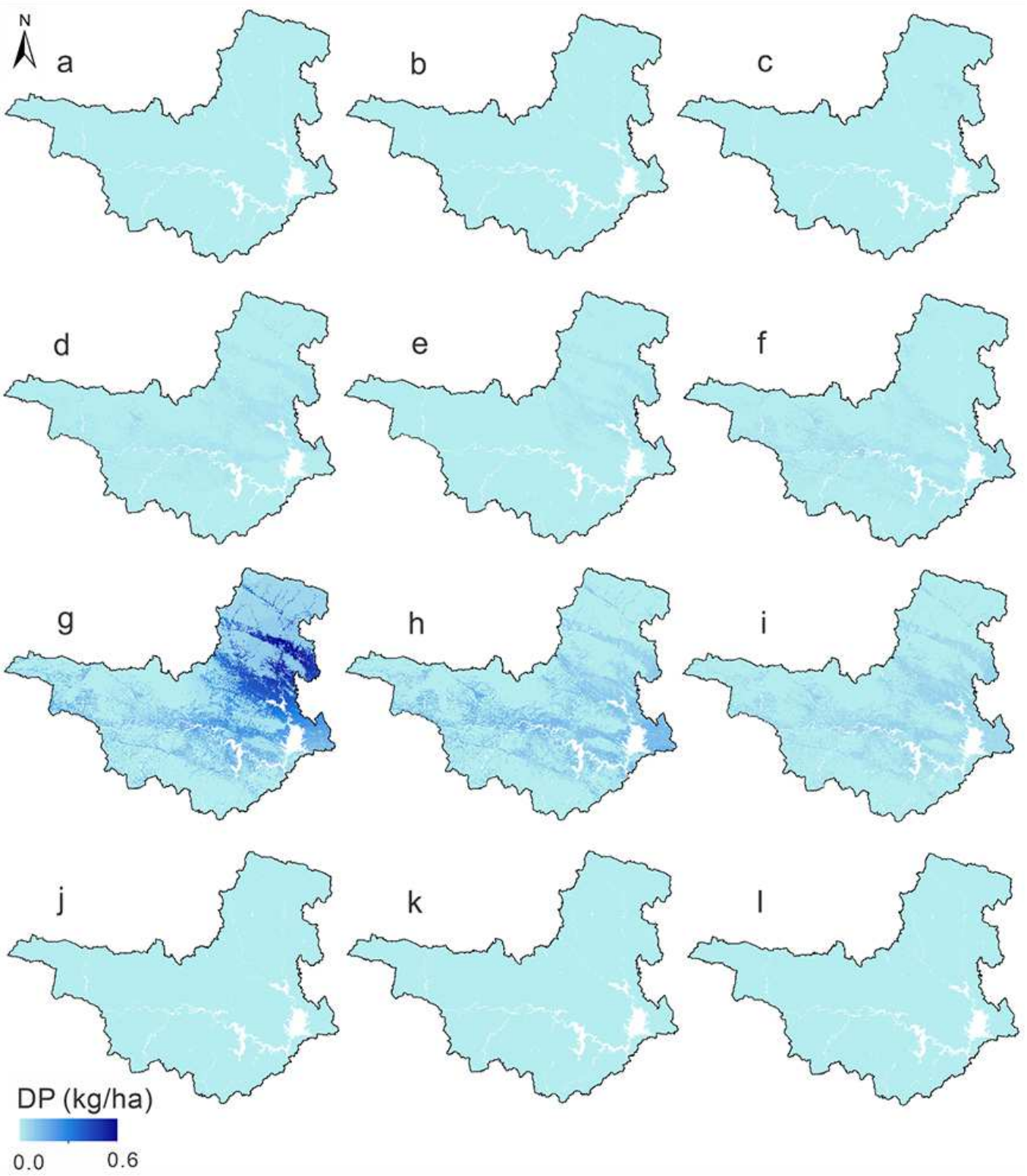

Figure 8

Distribution of unit dissolved phosphorus (DP) load (kg/ha) in DRB in 2010: (a) to (l) represent January to December (in the Appendix) Note: The designations employed and the presentation of the material on this map do not imply the expression of any opinion whatsoever on the part of Research Square concerning the legal status of any country, territory, city or area or of its authorities, or concerning the delimitation of its frontiers or boundaries. This map has been provided by the authors.

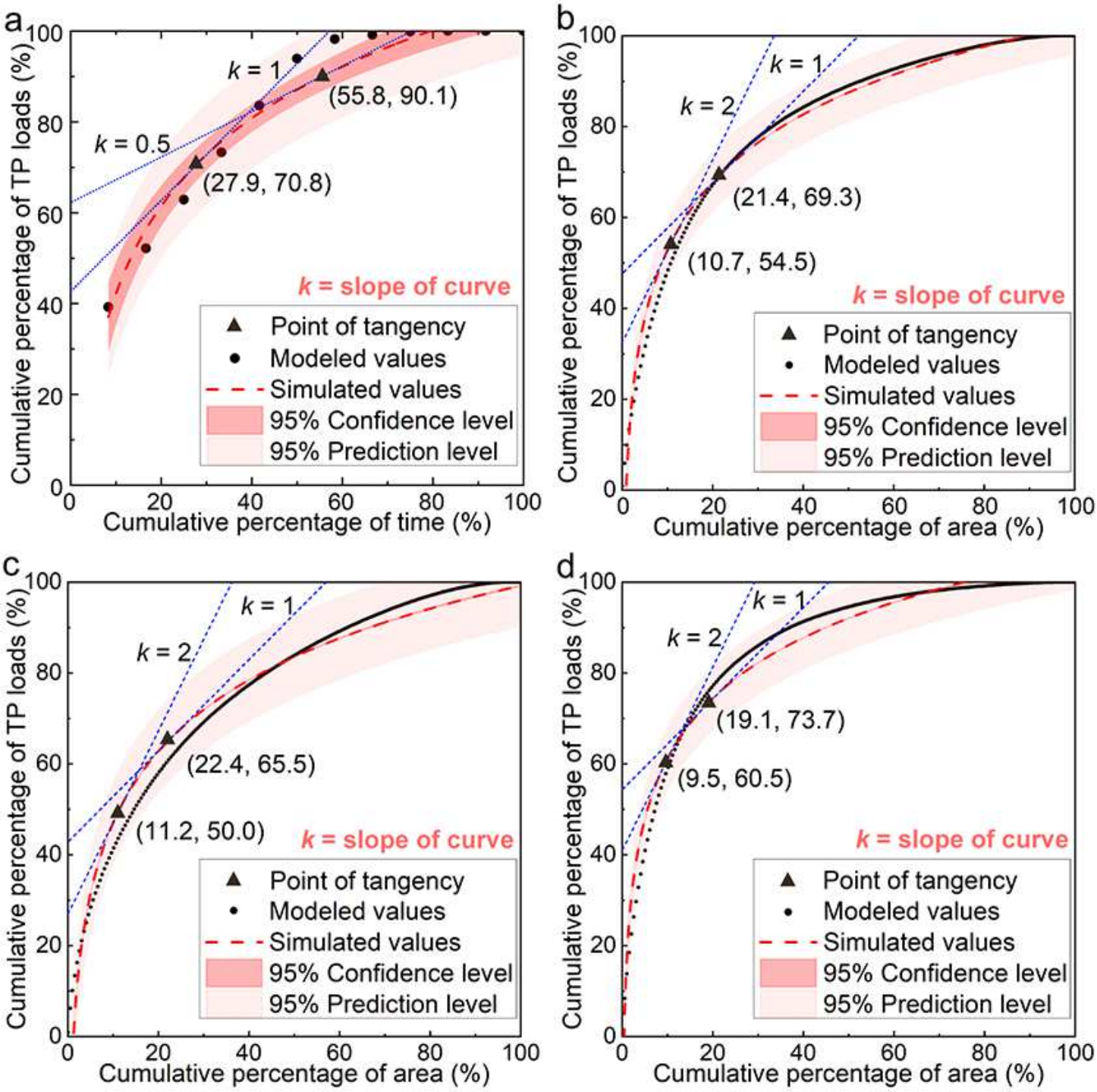

Figure 9

Cumulative load–time fitting curve (a) and cumulative load–area fitting curves (b–d): (a) cumulative load–time curve; (b) cumulative load–area curve of CSAs in CPs; (c) cumulative load–area curve of CSAs in sub-CPs; and (d) cumulative load–area curve of CSAs in non-CPs

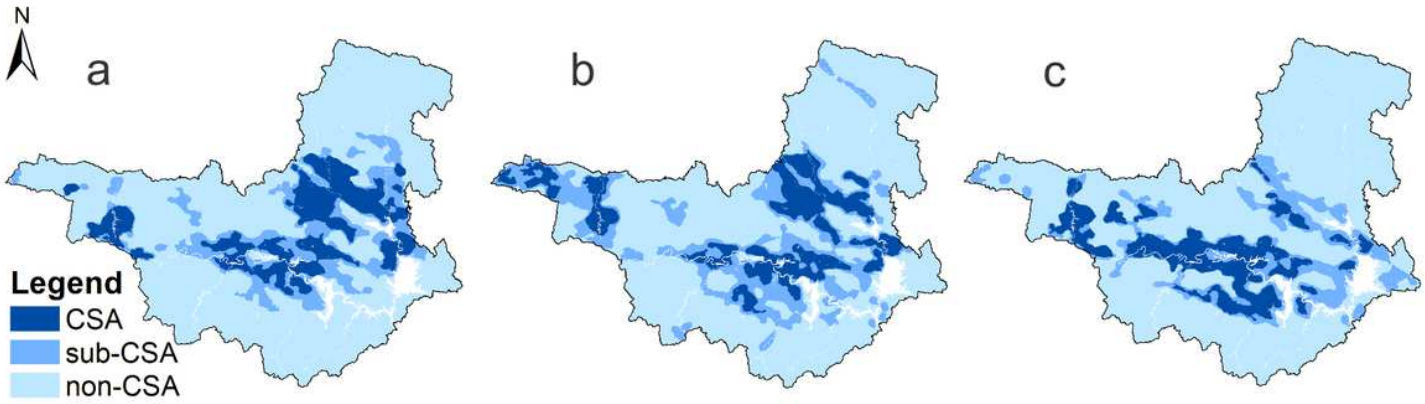

Figure 10

Spatial distribution of CSAs during different periods: (a) in CPs; (b) in sub-CPs; and (c) in non-CPs Note: The designations employed and the presentation of the material on this map do not imply the expression of any opinion whatsoever on the part of Research Square concerning the legal status of any country, territory, city or area or of its authorities, or concerning the delimitation of its frontiers or boundaries. This map has been provided by the authors.

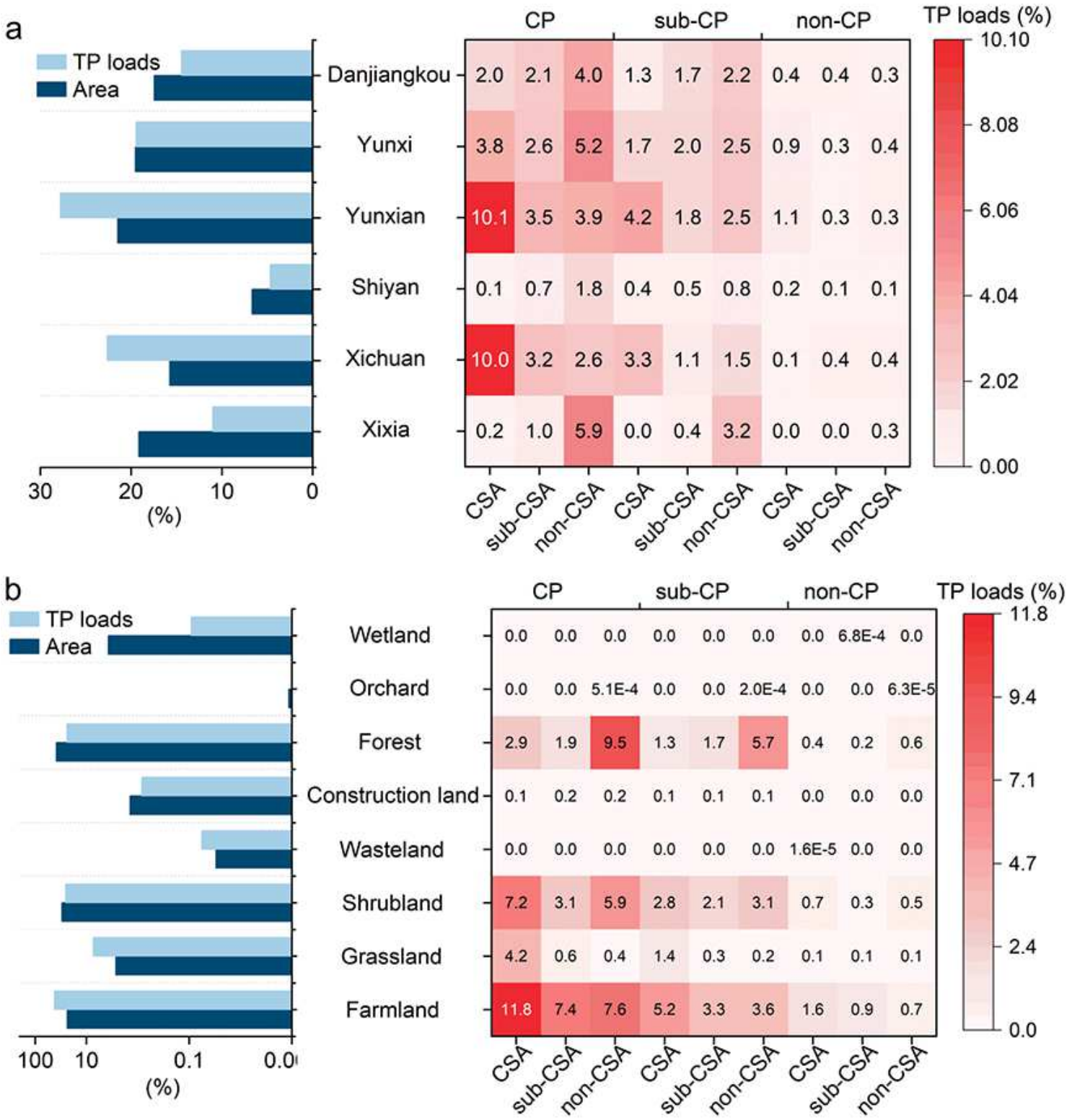

Figure 11

Proportion of TP loads in different periods and areas: (a) within each county and (b) within each land-use type